Journal of Alloys and Compounds 509 (2011) 6720–6724

Contents lists available at ScienceDirect

Journal of Alloys and Compounds

journal homepage: www.elsevier.com/locate/jallcom

Facile hydrothermal synthesis of CeO_2 nanosheets with high reactive exposure surface

Bo Liu[a], Quanjun Li[a], Xiaobo Du[b], Bingbing Liu[a,*], Mingguang Yao[a], Zepeng Li[a], Ran Liu[a], Dedi Liu[a], Xu Zou[a], Hang Lv[a], Dongmei Li[a], Bo Zou[a], Tian Cui[a], Guangtian Zou[a]

[a] State Key Laboratory of Superhard Materials, Jilin University, Changchun 130012, China
[b] College of Physics, Jilin University, No. 2699 Qianjin Street, Changchun 130012, China

ARTICLE INFO

Article history:
Received 28 December 2010
Received in revised form 25 March 2011
Accepted 28 March 2011
Available online 5 April 2011

Keywords:
Ceria
Nanosheet
(1 1 0)-dominant surface
Inorganic synthesis
One step

ABSTRACT

CeO_2 nanosheets with (1 1 0) dominated surface were synthesized for the first time by a facile one-step hydrothermal method without the assistance of any surfactant or template. The role of $NH_3{\cdot}H_2O$ on tailoring the morphology of CeO_2 nanocrystals was investigated. It was found the $NH_3{\cdot}H_2O$ not only serves as the precipitant, but also acts as structural direction agent in the formation of (1 1 0)-dominated CeO_2 nanosheets. Raman and XRD spectra showed that the sample has a cubic fluorite structure. Compared with bulk CeO_2 materials, the prepared CeO_2 nanosheets exhibit an obvious blue-shift in UV absorbance. The increase of the direct band gap energy of the obtained sample exceeds 8%. This method provides an environmentally friendly way for preparing CeO_2 nanostructures and tailoring their morphology. It may also be extended to the synthesis of other nanomaterials.

1. Introduction

As one of the most reactive rare earth materials, CeO_2 has attracted a great deal of attention due to its extensive applications in ultraviolet (UV) blockers, abrasives, catalysts, solid oxide fuel cells, gates for metal-oxide semiconductor devices and phosphors, etc. [1–5]. Nanostructured CeO_2 possesses superior physical and chemical properties compared with its bulk counterparts [6–8]. Over the years, remarkable progresses have been made in the study of the synthesis of CeO_2 nanomaterials with various morphologies and in the investigation of their corresponding novel properties [9–11].

Recently, a few researchers began to explore the influences of exposed surface structure on catalytic property of CeO_2 nanomaterials. Sayle et al. theoretically predicted that the (1 1 0) surface exhibits a more reactive tendency in the oxidation of CO than (1 1 1) surface due to its ready formation of oxygen vacancies [12]. Conesa et al. further discovered it is much easier to form oxygen vacancies on (1 0 0) plane, thus showing the high catalytic reactivity of ceria [13]. These theoretical results strongly suggest that the exposure of more reactive (1 1 0) and (1 0 0) surfaces will drastically enhance ceria's catalytic properties. Consequently, to elevate the catalytic activity of CeO_2 nanocrytals, tuning the ceria crystal shape to expose reactive crystal planes becomes an important scheme in the synthesis process. But, up to now, there were only a few groups attempted to synthesis CeO_2 nanocrystals with more reactive exposed surfaces. Yan et al. obtained high reactive CeO_2 nanorods with end faces of (1 1 0) and (1 0 0) planes together, using a hydrothermal method [14]. However, the uniformity and dispersity of the samples need to further improved. Besides, to clearly demonstrate the influence of reactive exposed surface on the catalytic property, it is necessary to have CeO_2 nanocrystals dominantly bounded by certain crystal plane. More recently, Adschiri et al. successfully synthesized well-dispersed CeO_2 nanocubes with (1 0 0) terminated surface using a supercritical hydrothermal process [15]. But, to tailor the surface structure in such a process, organic additive is required, high temperature (400 °C) is needed, and precursor must be obtained before the synthesis process. Hence, it remains a great challenge to synthesize high reactive CeO_2 nanocrystals of high quality having uniform size, well-defined crystal shape, and free of surfactants in a simple and economical one-step process. In addition, the (1 1 0) plane is also expected to strongly affect the catalytic activity [12,13]. However, to the best of our knowledge (1 1 0)-dominated CeO_2 nanocrystals have not been obtained by experiment so far, because (1 1 0) crystal plane has the highest surface energy state in the cubic symmetry nanocrystals.

Here, we report for the first time the preparation of CeO_2 nanosheets with (1 1 0)-dominated surface by a facile hydrothermal method. In the synthesis process, $NH_3{\cdot}H_2O$ was used to tailor

* Corresponding author. Tel.: +86 431 85168256; fax: +86 431 85168256.
E-mail address: liubb@jlu.edu.cn (B. Liu).

0925-8388/$ – see front matter
doi:10.1016/j.jallcom.2011.03.156

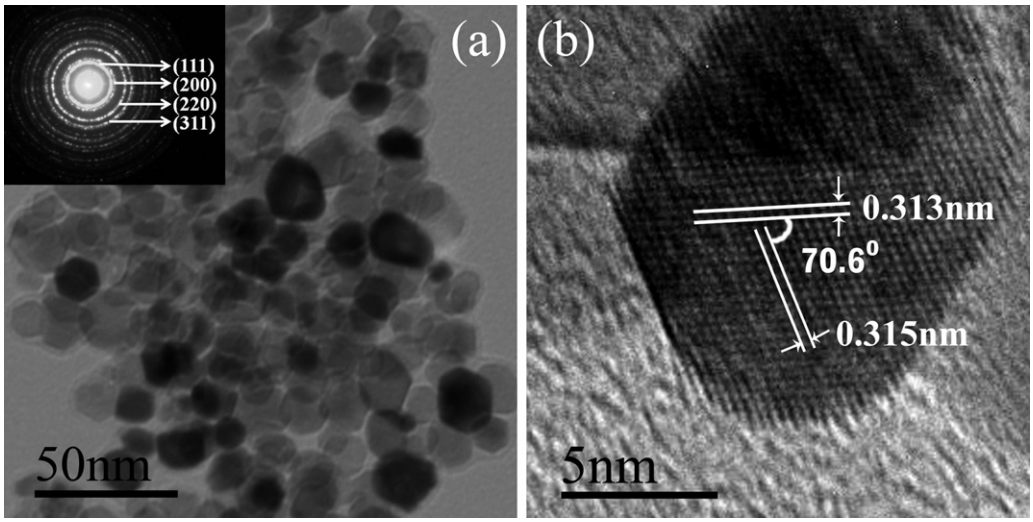

Fig. 1. (a) TEM image and ED pattern (insert in (a)) of the synthesized sample. (b) HRTEM image of the typical sample.

the surface structure of the sample without any surfactants or requiring any precursor. It is a one-step process without using organic additives. Hence, it is an environmentally friendly method for making advanced nanomaterials and devices. Our study shows that $NH_3{\cdot}H_2O$ has critical influences on the dispersity and morphology of the sample and our method is an effective approach to controlling CeO_2 morphology which may be extended to synthesis of other nanomaterials.

2. Experimental details

All the reactants used were of analytical grade without any further purification before the synthesized process. A Teflon-lined stainless steel cylindrical closed chamber with 50 mL capacity was used to synthesize the CeO_2 nanocrystals. In a typical synthesis, 1 mmol $Ce(NO_3)_3{\cdot}6H_2O$ was dissolved in 40 mL distilled water, and 1 mL $NH_3{\cdot}H_2O$ was injected into the transparent solution. Then the mixture was loaded into the Teflon-lined chamber. The autoclave was sealed and placed into an oven. It was maintained at 220 °C for 24 h and then cooled to room temperature naturally. The resulting light yellow precipitates were separated by centrifuging, washed with distilled water and ethanol several times respectively. Then, the final product was dried in air at 60 °C for 12 h and was collected for further characterization.

The (HITACHI H-8100) transmission electron microscope (TEM) with accelerating voltage of 200 kV and high-resolution transmission electron microscope (HRTEM, H-7500) were employed to analyze the typical product. X-ray powder diffraction (XRD) was used to characterize the product using Cu Kα radiation ($\lambda = 0.15418$ nm) with a scanning rate of 0.02° s^{-1} and a scanning range of 10–90°. The chemical composition of the sample was assessed with energy dispersive analysis of X-ray (EDAX CDU) by EDAX ZAF Quantification. The sample's Raman spectrum was obtained using the radiation of 514.5 nm from a Renishaw inVia Raman spectrometer. Its UV–vis spectrum was recorded using a UV-3150 spectrophotometer with a quartz cell (1 cm path length). The as-prepared powder was dispersed in ethanol at a concentration of around 0.2 g L^{-1}. It was sonicated at room temperature for 10 min to obtain a transparent colloidal solution. Ethanol was taken into account for blank. The optical absorption coefficient α was calculated according to the following equation: $\alpha = 2303A\rho/lc$, where A is the absorbance of the sample, ρ is the real density of CeO_2 (7.28 g cm^{-3}), l is the path length of the quartz cell (1 cm), and c is the concentration of the ceria suspensions.

3. Results and discussion

The morphology and structure of the CeO_2 nanosheets were characterized by TEM and electron diffraction (ED) techniques. Fig. 1(a) reveals that the synthesized sample possesses hexangular sheet-like morphology. The sample is well dispersed with the average size of 15 nm. ED pattern (inset in Fig. 1(a)) confirms the product is crystalline with cubic fluorite structure. The surface structure was analyzed by HRTEM. Fig. 1(b) represents the HRTEM image of a typical sample. The well defined 2D lattice planes are clearly shown in Fig. 1(b). The lattice planes with d-spacing of 0.315 and 0.313 nm both correspond to (1 1 1) planes. The angle between the two (1 1 1) planes is about 70.6°. According to crystal geometry, the common perpendicular plane of the two (1 1 1) planes is (1 1 0) plane. Therefore, the surface of the sample is dominated by (1 1 0) crystal planes. In previous theoretical works, (1 1 0) crystal plane is proven to have the highest surface energy and exhibit more catalytic activity for CO oxidation [12,13].

To study the crystal structure of the synthesized hexangular CeO_2 nanosheets, we carried out XRD measurement. Fig. 2 exhibits the typical XRD pattern of the synthesized hexangular CeO_2 nanosheets. All the detectable peaks in the pattern can be indexed to the pure cubic fluorite CeO_2 with a lattice constant $a = 0.5414$ (2) nm (JCPDS Card NO. 81-0792). This value

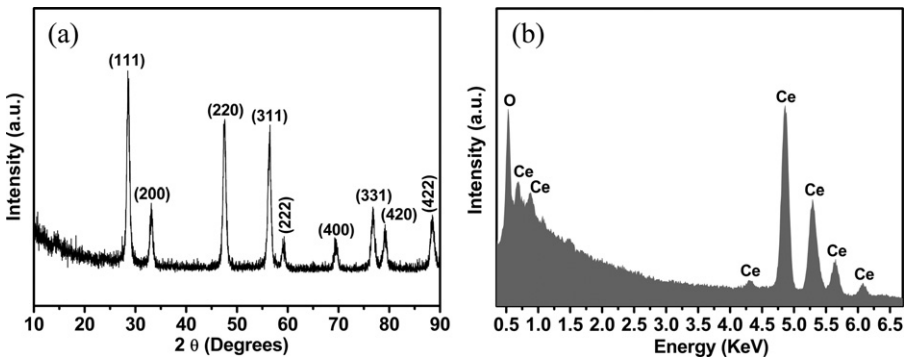

Fig. 2. (a) XRD pattern of the synthesized hexangular CeO_2 nanosheets. (b) EDAX spectrum of the synthesized hexangular CeO_2 nanosheets.

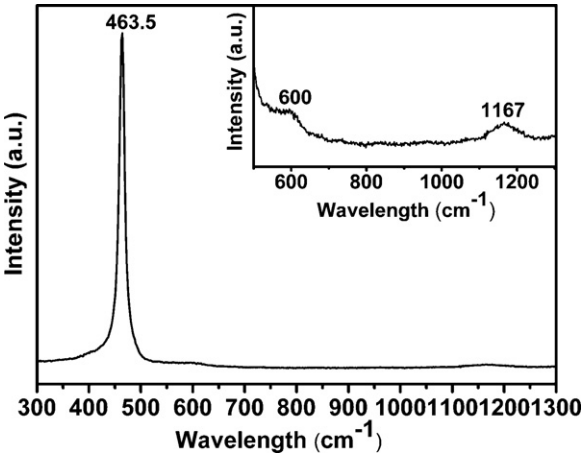

Fig. 3. Raman spectrum of the prepared CeO_2 nanocrystallines.

is in good agreement with the previous result of nanocrystals [16]. Using Debye-Scherrer formula, the strongest peaks (1 1 1) at $2\theta = 28.549^\circ$, (2 0 0) at $2\theta = 33.104^\circ$, (2 2 0) at $2\theta = 47.496^\circ$, and (3 1 1) at $2\theta = 56.379^\circ$ were used to calculate the average grain size of the hexangular CeO_2 nanocrystallines. It was determined to be around 15 nm. These results are consistent with that obtained by TEM and ED analysis. No crystalline impurity was detected from the XRD spectrum. To access chemical composition of the typical sample, EDAX was carried out. Fig. 2b shows the EDAX spectrum of the synthesized hexangular CeO_2 nanosheets. It confirms that there are only cerium and oxygen elements in the sample, and that the experimental stoichiometric index of Ce and O is 1 and 2.1 respectively, consistent with nominal stoichiometric index of CeO_2. From the above analysis, we have shown that the hexangular CeO_2 nanosheets obtained with our current method were of high purity of cubic fluorite-type structure.

We have also used Raman spectroscopy to further elucidate the structure of the synthesized sample. CeO_2 has a cubic fluorite-type structure and belongs to the O^5_h ($F\ m\ 3\ m$) space group. There is only one triply degenerate Raman active optical phonon (F_{2g}), which gives only one first order Raman line at about 465 cm^{-1}. In the second order Raman spectrum, overtones of this and of the zone boundary phonons as well as combinations and differences frequencies at each wave vectors q are allowed. With nine phonon branches, there are 45 tow phonon modes possible [17]. Fig. 3 shows the Raman spectrum of the prepared CeO_2 nanocrystallines. The synthesized sample exhibits only one first order Raman peak ($\sim$463.5 cm^{-1}), which can be assigned to F_{2g} symmetry. The second order Raman peaks are 600, 1167 cm^{-1} (insert in Fig. 3). These results are consistent with previous studies of pure cubic fluorite CeO_2 nanomaterials [18]. Thus, the Raman spectrum further confirms the formation of the fluorite-type structure in the synthesized CeO_2 nanosheets.

In the hydrothermal process, $NH_3{\cdot}H_2O$ was used in the synthesis of the CeO_2 nanocrystals. In order to clarify the key role of $NH_3{\cdot}H_2O$ in the formation of the hexangular CeO_2 nanosheets, the samples prepared at different concentrations of $NH_3{\cdot}H_2O$ were collected and characterized by TEM and ED techniques. Remarkably, without the addition of $NH_3{\cdot}H_2O$, no product can be obtained. When 0.5 mL $NH_3{\cdot}H_2O$ was added, the resulting product exhibited random agglomeration (Fig. 4(a)). ED pattern (inset in Fig. 4(a)) confirms the product is cubic fluorite type CeO_2, but with poor crystallinity. Increasing the content of $NH_3{\cdot}H_2O$ to 0.75 mL, hexangular CeO_2 nanocrystals started to emerge, but the main product was still random agglomeration (Fig. 4(b)). When $NH_3{\cdot}H_2O$ was increased to 1 mL, the main product exhibited hexangular sheet-like morphol-

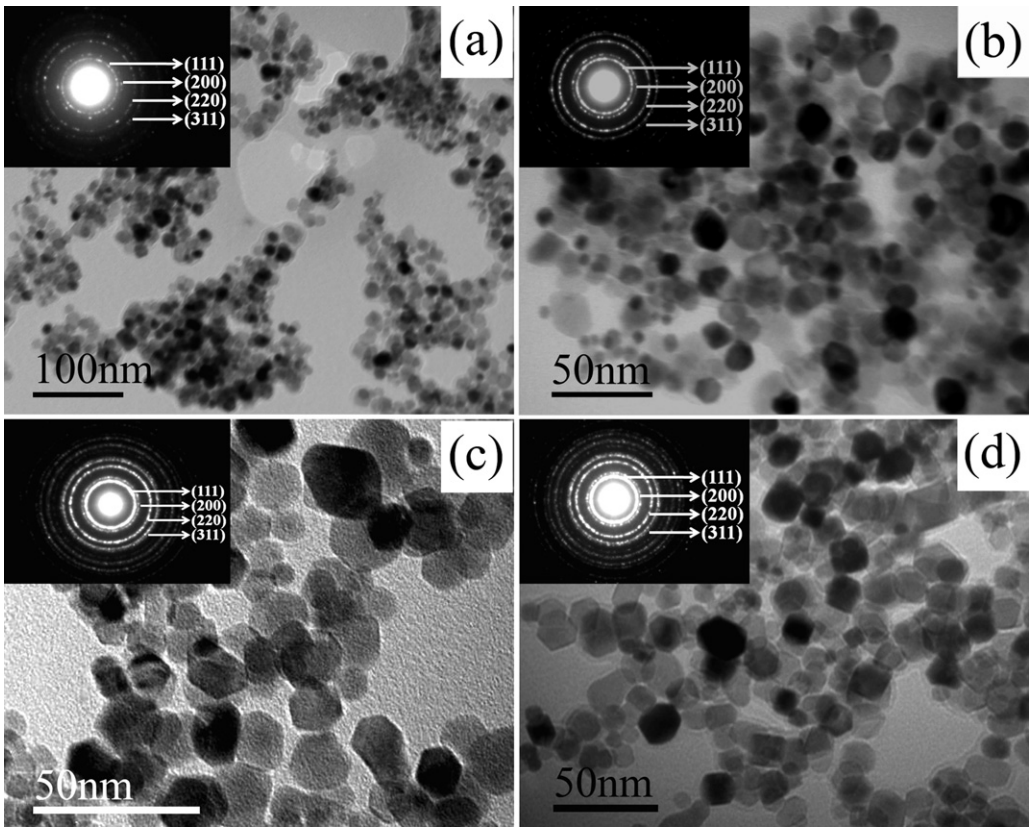

Fig. 4. TEM imagines and ED patterns (insert) of the samples collected at different contents of $NH_3{\cdot}H_2O$: (a) 0.5 mL; (b) 0.75 mL; (c) 1.0 mL; (d) 3.0 mL.

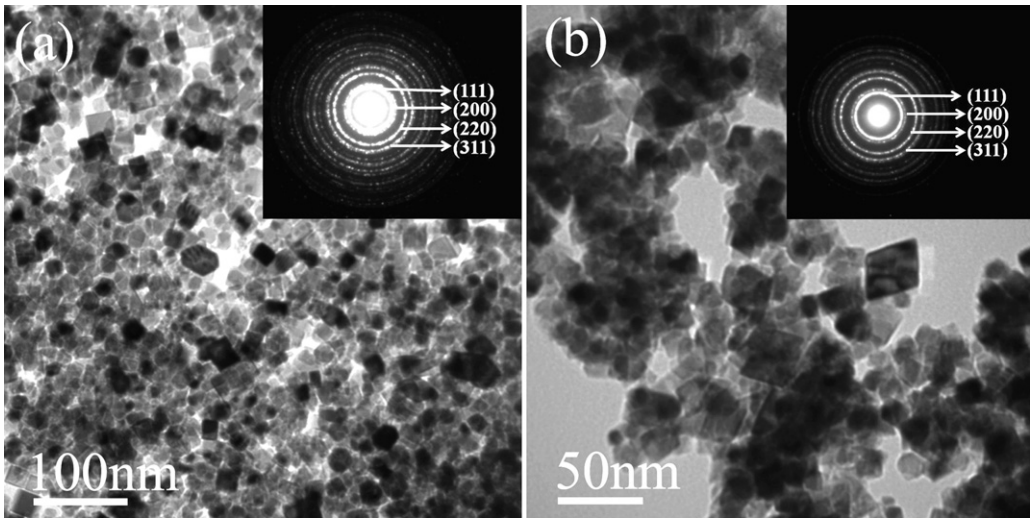

Fig. 5. TEM images and ED patterns (inset) of CeO_2 samples using different additives instead of $NH_3{\cdot}H_2O$: (a) NaOH; (b)Na_2CO_3.

ogy, with an average size of 15 nm (Fig. 4(c)). Further increasing the content of $NH_3{\cdot}H_2O$ to 3 mL, the sample almost keeps hexangular nano-sheets. The increase of $NH_3{\cdot}H_2O$ in the synthesized process appears to improve the crystal quality of the products. From the above analysis, we believe that $NH_3{\cdot}H_2O$ acts as a precipitant in the synthesis of hexangular CeO_2 nanosheets. At the early stage in the hydrothermal conditions, $NH_3{\cdot}H_2O$ hydrolysis gives rise to OH^- ions and NH^{4+} ions. Under basic conditions, the solubility product is much higher than the solubility constant, meaning the supersaturation value (S) is very large [19].

$$S = \frac{[Ce^{3+}][OH^-]^3}{K_{SP}}$$

where K_{SP} is the solubility constant of $Ce(OH)_3$, $[Ce^{3+}][OH^-]^3$ is the solubility product of the solution.

A high supersaturation value, S, establishes an environmental condition that favors homogeneous nucleation of $Ce(OH)_3$, which was then oxidized by O_2 existing in the reaction vessel and formed CeO_2. The reaction mechanism may be expressed:

$$Ce^{3+} + 3OH^- \rightarrow Ce(OH)_3 \quad (1)$$

$$4Ce(OH)_3 + O_2 \rightarrow 4CeO_2 + 6H_2O \quad (2)$$

In order to further confirm the indispensable function of $NH_3{\cdot}H_2O$ on tailoring the morphology of CeO_2 nanocrystals, some comparative experiments were performed. In the comparative experiments, $NH_3{\cdot}H_2O$ was substituted by NaOH or Na_2CO_3, while other synthetic parameters were kept the same as those in the typical synthesis. Fig. 5 shows the TEM and ED patterns of the products obtained in the comparative experiments. When NaOH or Na_2CO_3 was used instead of $NH_3{\cdot}H_2O$, no regular morphologies could be observed and the resulting products agglomerate randomly. ED patterns show both of the products are cubic fluorite-type CeO_2 nanocrystals. On the basis of the above results of the comparative experiments we infer that $NH_3{\cdot}H_2O$ may have structural direction

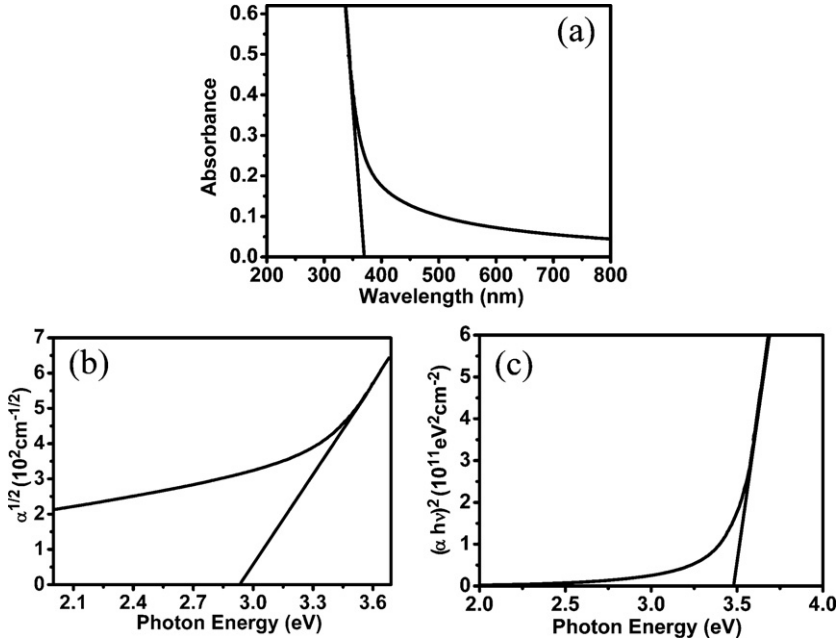

Fig. 6. (a) UV spectrum for synthesized CeO_2 nanosheets; (b) plot of $\alpha^{1/2}$ vs photon energy for synthesized CeO_2 nanosheets; (c) plot of $(\alpha h\upsilon)^2$ vs photon energy for synthesized CeO_2 nanosheets.

effect in the formation of the CeO_2 nanosheets, similar to that of $NH_4H_2PO_4$ in the formation of Fe_2O_3 nanotubes and Na_3PO_4 in the synthesis of CeO_2 nano-octahedrons [20,21].

Ceria is a very attractive material as an ultraviolet absorbent, with the strongest absorption at about 400 nm. Recently, extensive research has shown that UV light in the UV-A spectra range (310–400 nm) accelerates photosynthesis in the plants and activates an enzyme which restores damaged DNA, whereas the light in the range between 310 and 210 nm (UV-B and UV-C) does damages to living things [22]. Therefore, it is useful to control the position of the UV absorption edge, so as to transmit some of the UV-A light. Optical properties of the typical sample were characterized by UV absorption spectrum. Fig. 6(a) shows the typical absorption spectrum of the synthesized CeO_2 nanocrystals. A strong absorption at about 370 nm can be observed for the typical sample, which exhibits 30 nm blue-shift relative to the bulk materials (400 nm). The obvious UV-absorption for ceria originates from charge-transfer between the O*2p* and Ce*4f* states in O^{2-} and Ce^{4+} [23]. For indirect interband transitions, α near the absorption edge can be expressed in the following equation [24]:

$$\alpha \propto \frac{(h\upsilon + E_p - E_i)^2}{(e^{h\upsilon/\kappa T} - 1)} + \frac{(h\upsilon - E_p - E_i)^2 e^{h\upsilon/\kappa T}}{(e^{h\upsilon/\kappa T} - 1)}$$

where E_i is the band gap energy for indirect transitions, E_p the phonon energy, κ_i the Boltzmann constant, $h\upsilon$ the photon energy, and T the absolute temperature. The plot of $\alpha^{1/2}$ vs photon energy of CeO_2 nanosheets is shown in Fig. 6(b). The intersection of the extrapolated linear portion gives the indirect band gap energy (E_i). The E_i value of the CeO_2 nanosheets was obtained as 2.90 eV. The value is consistent with the previous study of CeO_2 nanoparticles [25]. For direct transitions, α near the absorption edge can be expressed in the following equation [24]:

$$\alpha \propto \frac{(h\upsilon - E_d)^{1/2}}{h\upsilon}$$

where E_d is the band gap energy for direct transitions. The plot of $(\alpha h\upsilon)^2$ vs photon energy of the CeO_2 nanosheets is shown in Fig. 6(c). From the intersection of the extrapolated linear portion, the E_d value of the CeO_2 nanosheets is determined as 3.45 eV. Compared with pure bulk crystal (E_d = 3.19 eV) [25], the increase of the direct band gap energy of CeO_2 nanocrystals exceeds 8%. The larger blue-shift of the CeO_2 nanosheets may contribute to quantum size effect [26]. Therefore, the synthesized hexangular CeO_2 nanosheets are useful materials which can block harmful ultraviolet rays.

4. Conclusions

In summary, we synthesized (1 1 0)-dominated CeO_2 nanosheets using a facile one-step hydrothermal method. In the typical hydrothermal process, $NH_3{\cdot}H_2O$ plays a critical role in tailoring the surface structure of the CeO_2 nanocrystals without the assistance of any surfactant or template. The key function of the $NH_3{\cdot}H_2O$ on tailoring the morphology of CeO_2 nanocrystals was investigated. The results show that the $NH_3{\cdot}H_2O$ not only serves as the precipitant, but also acts as the structural direction agent in the formation of (1 1 0)-dominated CeO_2 nanosheets. Raman and XRD spectra show that the sample is pure cubic fluorite structure. Compared with bulk CeO_2 materials, the prepared CeO_2 nanosheets exhibit an obvious blue-shift in UV absorbance. The direct band gap energy of the obtained sample increases more than 8%. Its special property of UV absorption makes it an excellent candidate for ultraviolet blockers.

Acknowledgements

This work was supported financially by the NSFC (10979001, 51025206, 51032001, 21073071, 11004075, 11074090), the National Basic Research Program of China (2011CB808200), the Cheung Kong Scholars Programme of China.

References

[1] A.A. Ansari, S.P. Singh, B.D. Malhotra, J. Alloys Compd. 509 (2011) 262–265.
[2] L.-S. Zhong, J.-S. Hu, A.-M. Cao, Q. Liu, W.-G. Song, L.-J. Wan, Chem. Mater. 19 (2007) 1648–1655.
[3] A.A. Athawale, M.S. Bapat, P.A. Desai, J. Alloys Compd. 484 (2009) 211–217.
[4] B.-H. Lee, T. Nakayama, Y. Tokoi, T. Suzuki, K. Niihara, J. Alloys Compd. 509 (2011) 1231–1235.
[5] S. Li, Z. Li, B. Bergman, J. Alloys Compd. 492 (2010) 392–395.
[6] B.B. Patil, S.H. Pawar, J. Alloys Compd. 509 (2011) 414–420.
[7] G. Chen, C. Xu, X. Song, S. Xu, Y. Ding, S. Sun, Cryst. Growth Des. 8 (2008) 4449–4453.
[8] S. Kim, J.S. Lee, C. Mitterbauer, Q.M. Ramasse, M.C. Sarahan, N.D. Browning, H.J. Park, Chem. Mater. 21 (2009) 1182–1186.
[9] R. Yu, L. Yan, P. Zheng, J. Chen, X. Xing, J. Phys. Chem. C 112 (2008) 19896–19900.
[10] X. Liu, K. Zhou, L. Wang, B. Wang, Y. Li, J. Am. Chem. Soc. 131 (2009) 3140–3141.
[11] S.A. Hassanzadeh-Tabrizi, M. Mazaheri, M. Aminzare, S.K. Sadrnezhaad, J. Alloys Compd. 491 (2010) 499–502.
[12] T.X.T. Sayle, S.C. Parker, C.R.A. Catlow, Surf. Sci. 316 (1994) 329–336.
[13] J. Conesa, Surf. Sci. 339 (1995) 337–352.
[14] H.-X. Mai, L.-D. Sun, Y.-W. Zhang, R. Si, W. Feng, H.-P. Zhang, H.-C. Liu, C.-H. Yan, J. Phys. Chem. B 109 (2005) 24380–24385.
[15] J. Zhang, S. Ohara, M. Umetsu, T. Naka, Y. Hatakeyama, T. Adschiri, Adv. Mater. 19 (2007) 203–206.
[16] Y.-W. Zhang, R. Si, C.-S. Liao, C.-H. Yan, C.-X. Xiao, Y. Kou, J. Phys. Chem. B 107 (2003) 10159–10167.
[17] W.H. Weber, K.C. Hass, J.R. McBride, Phys. Rev. B 48 (1993) 178.
[18] J.E. Spanier, R.D. Robinson, F. Zhang, S.-W. Chan, I.P. Herman, Phys. Rev. B 64 (2001) 245407.
[19] X.D. Zhou, W. Huebner, H.U. Anderson, Appl. Phys. Lett. 80 (2002) 3814–3816.
[20] C.-J. Jia, L.-D. Sun, Z.-G. Yan, L.-P. You, F. Luo, X.-D. Han, Y.-C. Pang, Z. Zhang, C.-H. Yan, Angew. Chem. Int. Ed. 44 (2005) 4328–4333.
[21] L. Yan, R. Yu, J. Chen, X. Xing, Cryst. Growth Des. 8 (2008) 1474–1477.
[22] H.-S. Kang, J. Hidema, T. Kumagai, Photochem. Photobiol. 68 (1998) 71–77.
[23] S. Tsunekawa, R. Sahara, Y. Kawazoe, A. Kasuya, Mater. Trans. JIM 41 (2000) 1104–1107.
[24] X. Lu, X. Li, F. Chen, C. Ni, Z. Chen, J. Alloys Compd. 476 (2009) 958–962.
[25] S. Tsunekawa, T. Fukuda, A. Kasuya, J. Appl. Phys. 87 (2000) 1318–1321.
[26] C. Ho, J.C. Yu, T. Kwong, A.C. Mak, S. Lai, Chem. Mater. 17 (2005) 4514–4522.